J. Fluid Mech. (2012), *vol.* 694, *pp.* 524–539.
doi:10.1017/jfm.2012.7

Inviscid instability of a stably stratified compressible boundary layer on an inclined surface

Julien Candelier[1,2], Stéphane Le Dizès[2]† and Christophe Millet[1]

[1] CEA, DAM, DIF, F-91297 Arpajon, France

[2] IRPHE, CNRS & Aix-Marseille University, 49 rue F. Joliot-Curie, F-13013 Marseille, France

(Received 21 March 2011; revised 12 December 2011; accepted 27 December 2011; first published online 2 February 2012)

The three-dimensional stability of an inflection-free boundary layer flow of length scale L and maximum velocity U_0 in a stably stratified and compressible fluid of constant Brunt–Väisälä frequency N, sound speed c_s and stratification length H is examined in an inviscid framework. The shear plane of the boundary layer is assumed to be inclined at an angle θ with respect to the vertical direction of stratification. The stability analysis is performed using both numerical and theoretical methods for all the values of θ and Froude number $F = U_0/(LN)$. When non-Boussinesq and compressible effects are negligible ($L/H \ll 1$ and $U_0/c_s \ll 1$), the boundary layer flow is found to be unstable for any F as soon as $\theta \neq 0$. Compressible and non-Boussinesq effects are considered in the strongly stratified limit: they are shown to have no influence on the stability properties of an inclined boundary layer (when $F/\sin\theta \ll 1$). In this limit, the instability is associated with the emission of internal-acoustic waves.

Key words: boundary layer stability, stratified flows

1. Introduction

Tollmien–Schlichting waves are viscous perturbations which are usually responsible for the destabilization of inflection-free boundary layers such as the Blasius boundary layer. These unstable waves do not exist in an inviscid framework. However, in the presence of stratification or compressibility, inflection-free boundary layer flows can become unstable with respect to new inviscid instability modes. The goal of the present study is to analyse the characteristics of such instability modes. We also want to understand the effect of the inclination angle between the shear plane and the direction of stratification on the stability properties.

The inviscid stability properties of boundary layers have been mainly studied in two frameworks: supersonic flows and geophysical flows. When the fluid is compressible, Mack (1969) explains that as soon as the flow becomes supersonic, there is an additional sequence of modes. These additional modes were called higher modes when first discovered by Mack (1965), in order to distinguish them from the mode that

† Email address for correspondence: ledizes@irphe.univ-mrs.fr

had been studied by Dunn & Lin (1955) and Lees & Reshotko (1962). At low Mach numbers, this mode, called the first mode, represents the extension to compressible flow of Tollmien–Schlichting (TS) waves. But as the Mach number approaches three for adiabatic boundary layers, the viscous instability mechanism that is responsible for TS waves vanishes, while unstable first-mode waves persist. In this Mach number regime, the mechanism of instability of the first mode is inviscid and corresponds to the extension in the presence of the temperature gradient of the Rayleigh inflectional criterion (Lees & Lin 1946). The instability mechanism of higher modes is different and associated with wave radiation, and for this reason the terminology 'acoustic modes' has often been used (see discussion in Mack 1990). These unstable modes have also been found in confined mixing layers (Tam & Hu 1989*a*), in compressible two-dimensional jets (Mack 1990), in supersonic round jets (Tam & Hu 1989*b*; Luo & Sandham 1997; Parras & Le Dizès 2010), and in vortices (Broadbent & Moore 1979; Kopev & Leontev 1983).

In stratified fluids, most studies have considered configurations where shear and stratification are aligned in the same direction. Moreover, they have mainly been concerned with the effects of stratification on the shear instability in relation with the Richardson criterion for instability (Howard 1961; Miles 1961). However, the presence of a ground was also shown to create other less unstable modes (Davis & Peltier 1976; Mastrantonio *et al.* 1976). The mechanism of instability associated with over-reflection was further analysed by Lindzen & Barker (1985) and Smyth & Peltier (1989), among others. Although the presence of an inflection point is not a necessary condition for instability when a solid ground is present (Chimonas 1974), inflection-free profiles have been found to be generally stable on the inviscid basis (Chimonas 2002). Only combinations of inflection-free profiles with abrupt density variations have been shown possibly to lead to instability (Churilov 2005, 2008). Nevertheless, the waves which are often observed in atmospheric boundary layers are not easily explained by such mechanisms. In the present work, we shall provide an alternative explanation where the instability comes from the angle that shear and stratification could make with each other. In the final discussion, we shall show that this instability could be active in nocturnal atmospheric boundary layers when the angle exceeds 20°.

We shall analyse both stratification and compressible effects by considering the idealized configuration of a hyperbolic tangent profile with constant Brunt–Väisälä frequency N and constant sound speed c_s. The plane of the boundary layer will be assumed to be inclined at an angle θ with respect to the vertical direction of stratification. We shall see that when the boundary is inclined, the flow exhibits unstable radiative modes owing to the stratification. These radiative modes, whose unstable character is associated with the wave emission, are similar to the acoustic waves of compressible flow mentioned above. They have also been obtained in shallow water shear flows (see, for instance, Satomura 1981; Takehiro & Hayashi 1992; Ford 1994; Balmforth 1999; Dritschel & Vanneste 2006). In a continuously stratified fluid, they have been found in columnar vortices (Schecter & Montgomery 2004; Billant & Le Dizès 2009; Le Dizès & Billant 2009; Riedinger, Le Dizès & Meunier 2010*a*; Riedinger, Meunier & Le Dizès 2010*b*), in rotating flows (Le Dizès & Riedinger 2010; Riedinger, Le Dizès & Meunier 2011) and in jets (Candelier 2010). The instability mechanism is directly related to the mechanism of over-reflection (Basovich & Tsimring 1984; Le Dizès & Billant 2009).

The paper is organized as follows. In § 2, the base flow and the perturbation equations are provided. Both compressible and non-Boussinesq effects are considered in the formulation. The strongly stratified limit (small F) is considered in § 3. In this

limit, we show that compressible and non-Boussinesq effects have no influence on the stability properties. In § 4, the weakly stratified limit (large F) is analysed. In § 5, general results are provided when compressible and non-Boussinesq effects are negligible. In the last section, an application to a stable nocturnal atmospheric boundary layer is discussed.

2. Base flow and perturbation equations

We consider a two-dimensional boundary layer flow in a stably stratified, compressible, non-rotating, inviscid fluid. The velocity field $\boldsymbol{u}_g$, pressure p_g, density ρ_g and potential temperature Θ_g of such a flow are assumed to be governed by the Euler equations

$$\frac{\mathrm{D}\boldsymbol{u}_g}{\mathrm{D}t} = -\frac{1}{\rho_g}\boldsymbol{\nabla} p_g - g\boldsymbol{e}_Z, \tag{2.1a}$$

$$\frac{\mathrm{D}\rho_g}{\mathrm{D}t} + \rho_g \boldsymbol{\nabla}\cdot\boldsymbol{u}_g = 0, \tag{2.1b}$$

$$\frac{\mathrm{D}\Theta_g}{\mathrm{D}t} = 0, \tag{2.1c}$$

and the perfect gas law

$$\Theta_g = \frac{p_g}{\rho_g R}\left(\frac{p_0}{p_t}\right)^{1-1/\gamma}, \tag{2.2}$$

where g is gravity, $\boldsymbol{e}_Z$ is the unit vector in the vertical direction, p_0 is a pressure of reference, R is the perfect gas constant and $\gamma = c_p/c_v$ is the ratio of specific heats.

The potential temperature $\overline{\Theta}(Z)$, pressure $\overline{p}(Z)$ and density $\overline{\rho}(Z)$ of the base flow are assumed to depend on the vertical coordinate Z (oriented upward) only. The fluid is then characterized by a sound speed c_s, a Brunt–Väisälä frequency N, and a stratification length H defined by

$$c_s^2 = \frac{\gamma\overline{p}}{\overline{\rho}}, \tag{2.3a}$$

$$N^2 = \frac{g}{\overline{\Theta}}\overline{\Theta}_Z, \tag{2.3b}$$

$$H = \frac{\overline{\Theta}}{\overline{\Theta}_Z}, \tag{2.3c}$$

where $\overline{\Theta}_Z$ is the derivative of the potential temperature with respect to Z. In the following, these three quantities are assumed to be constant. Note that the assumption of constant sound speed implies that the gas is isothermal.

The base flow velocity field is assumed to be given by

$$\overline{\boldsymbol{u}} = U(z)\boldsymbol{e}_x = U_0 \tanh(z/L)\boldsymbol{e}_x, \tag{2.4}$$

to mimic a boundary layer flow in a viscous fluid with no-slip boundary conditions. The flow is two-dimensional and defined above the boundary $z = 0$. The (x, z) shear plane of the base flow is assumed to make an angle θ with respect to the direction of stratification Z, as shown in figure 1. With this definition, $\theta = 0$ corresponds to the flow over a horizontal surface, whereas $\theta = \pi/2$ corresponds to the flow over a vertical surface. For any angle θ, the base flow is aligned with the isopycnals. Note also that the base flow velocity field does not possess any inflection point within the fluid. The

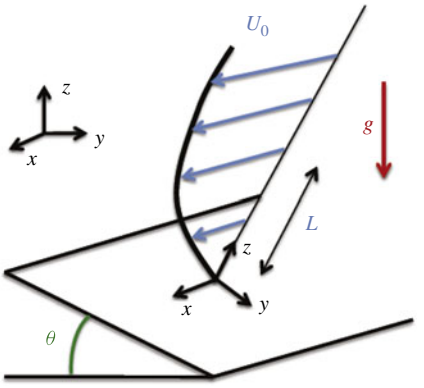

FIGURE 1. (Colour online available at journals.cambridge.org/flm) Sketch of the base flow and definition of the angle θ.

velocity field (2.4) with the pressure $\overline{p}$, density $\overline{\rho}$ and potential temperature $\overline{\Theta}$ defined above satisfy (2.1*a–c*) and (2.2). In the following, we consider perturbations to this base flow which satisfy slip boundary conditions at $z = 0$.

The velocities, lengths and pressure are non-dimensionalized by the maximal velocity U_0, the boundary layer scale L and $\rho_0 U_0^2$, respectively. The base flow is then characterized by four dimensionless parameters: the angle θ, the Froude number $F = U_0/(LN)$, the Mach number $M = U_0/c_s$ and the non-dimensional stratification length $\bar{H} = H/L$, from which it is useful to define the Eckart parameter $\Gamma = M^2\bar{H}/F^2 - 1/(2\bar{H})$ (see Eckart 1960). Typical values of these parameters for stable atmospheric boundary layers are $F = 0.1$–50, $M = 0.005$–0.1, $\bar{H} = 10$–1000 and $\Gamma = 0.001$–0.1.

Local temporal stability properties are obtained by considering perturbations of velocity $\boldsymbol{u}' = (u', v', w')$, pressure p', density ρ' and potential temperature Θ' as a plane wave

$$(\boldsymbol{u}', p', \rho', \Theta') = \overline{\rho}^{1/2}(\boldsymbol{u}, p/\overline{p}, \rho/\overline{\rho}, \Theta/\overline{\Theta}) \exp(\mathrm{i}k_x x + \mathrm{i}k_y y - \mathrm{i}\omega t), \tag{2.5}$$

where k_x and k_y are real wavenumbers in the streamwise and spanwise directions and $\omega = \omega_r + \mathrm{i}\omega_i$ is the complex frequency. The real part ω_r is the oscillation frequency and the imaginary part ω_i defines the growth rate. The perturbation equations are obtained by linearizing equations (2.1*a–c*) around the base flow defined by (2.3*a–c*) and (2.4). By taking into account that (2.2) implies $\Theta = M^2 p - \rho$, these equations can be written as

$$-\mathrm{i}\phi u + U_z w + \mathrm{i}k_x p = 0, \tag{2.6a}$$

$$-\mathrm{i}\phi v + \mathrm{i}k_y p - \Gamma \sin\theta p - \sin\theta b = 0, \tag{2.6b}$$

$$-\mathrm{i}\phi w + \frac{\mathrm{d}p}{\mathrm{d}z} + \Gamma \cos\theta p + \cos\theta b = 0, \tag{2.6c}$$

$$-\mathrm{i}\phi b + \frac{\sin\theta}{F^2} v - \frac{\cos\theta}{F^2} w = 0, \tag{2.6d}$$

$$-\mathrm{i}\phi M^2 p + \mathrm{i}k_x u + \mathrm{i}k_y v + \frac{\mathrm{d}w}{\mathrm{d}z} - \Gamma \sin\theta v + \Gamma \cos\theta w = 0, \tag{2.6e}$$

where $\phi = \omega - k_x U$ is the inertial frequency of the perturbation, U_z is the derivative with respect to z of the base flow velocity U, and $b = -(gL/U_0^2)\Theta$ is the amplitude

of the buoyancy perturbation. Thanks to the renormalization factor $\overline{\rho}^{1/2}$ in (2.5), the system (2.6) takes a symmetric form in which the Eckart parameter Γ appears as the natural quantity to measure non-Boussinesq effects in the presence of compressibility (for more explanations, see Gossard & Hooke 1975). Note that it is only when both compressible and non-Boussinesq effects are negligible ($M = \Gamma = 0$) that the perturbations satisfy $\mathrm{div}(\boldsymbol{u}) = 0$.

By eliminating u, v, w and b from (2.6), a single equation for p can be found:

$$(\bar{\phi}^2 - \sin^2\theta)\frac{\mathrm{d}^2 p}{\mathrm{d}z^2} + \left[-2\bar{\phi}_z\frac{(2\bar{\phi}^2-1)\sin^2\theta - \bar{\phi}^4}{\bar{\phi}(1-\bar{\phi}^2)} - 2\mathrm{i}k_y\sin\theta\cos\theta\right]\frac{\mathrm{d}p}{\mathrm{d}z} + \left[k_x^2(1-\bar{\phi}^2) + k_y^2(\cos^2\theta - \bar{\phi}^2) - 2\mathrm{i}k_y\bar{\phi}_z\sin\theta\cos\theta\frac{2\bar{\phi}^2-1}{\bar{\phi}(1-\bar{\phi}^2)} - 2\bar{\phi}_z\Gamma\cos\theta\frac{\bar{\phi}^3}{(1-\bar{\phi}^2)} - \Gamma^2\bar{\phi}^2 - M^2\phi^2(1-\bar{\phi}^2)\right]p = 0, \tag{2.7}$$

where $\bar{\phi} = \phi F$, $\bar{\phi}_z = -Fk_xU_z$. This equation is the extension in the presence of compressible and non-Boussinesq effects of the equation already derived in Candelier, Le Dizès & Millet (2011). In the absence of flow ($U = 0$), this equation possesses oscillatory solutions of the form $\exp(\mathrm{i}k_z z)$, where k_z is related to k_x, k_y and ω by the general dispersion relation of internal-acoustic waves. If we define vertical and horizontal wavenumbers as $k_v^2 = (k_z\cos\theta - k_y\sin\theta)^2$ and $k_h^2 = k_x^2 + (k_y\cos\theta + k_z\sin\theta)^2$, this dispersion relation can be written in a well-known form (see for instance Houghton 1986; Watada 2009):

$$k_v^2 = k_h^2\left(\frac{1}{\omega^2F^2} - 1\right) + M^2\left(\omega^2 - \frac{1}{F^2}\right) - \Gamma^2. \tag{2.8}$$

The boundary conditions to be applied to the pressure amplitude p are deduced from the condition that the normal velocity w should vanish at the boundary $z = 0$. Using (2.6), this condition gives

$$(\sin^2\theta - \omega^2F^2)\frac{\mathrm{d}p}{\mathrm{d}z} + (\mathrm{i}k_y\sin\theta\cos\theta + \Gamma F^2\omega^2\cos\theta)p = 0 \quad \text{at } z = 0. \tag{2.9}$$

Far away from the boundary, we assume that the perturbation propagates energy outward. Since the flow is uniform at infinity, far away from the boundary, the perturbation is a plane wave whose characteristics are defined by (2.8). The wave propagating energy outward can be obtained by the causality condition that it should be spatially damped outward when $\omega_i > 0$.

To solve this eigenvalue problem, we have used two different numerical techniques. We have either integrated (2.7) using a shooting method or solved the complete system (2.6) by a pseudo-spectral code which was already used in Riedinger *et al.* (2010*a*) and Candelier *et al.* (2011). We refer the readers to these papers for more details.

In the following, we first consider the limit cases where F is either small or large.

3. The strongly stratified limit (small F)

In this section, we consider the limit where both F and $F/\sin\theta$ are small. We then implicitly assume that the boundary layer is inclined ($\theta \neq 0$) in a

strongly stratified fluid. In this limit, it is convenient to consider the new function $q(z) = \exp(\mathrm{i}k_y z \cot\theta)p(z)$, which satisfies

$$(\bar{\phi}^2 - \sin^2\theta)\frac{\mathrm{d}^2 q}{\mathrm{d}z^2} + \left[-2\bar{\phi}_z\frac{(2\bar{\phi}^2-1)\sin^2\theta - \bar{\phi}^4}{\bar{\phi}(1-\bar{\phi}^2)} - 2\mathrm{i}k_y\frac{\cos\theta}{\sin\theta}\bar{\phi}^2\right]\frac{\mathrm{d}q}{\mathrm{d}z} + \left[k_x^2(1-\bar{\phi}^2) - \frac{k_y^2}{\sin^2\theta}\bar{\phi}^2 - 2\bar{\phi}_z\cos\theta\frac{\bar{\phi}^3}{(1-\bar{\phi}^2)}\left(\Gamma + \mathrm{i}\frac{k_y}{\sin\theta}\right) - \Gamma^2\bar{\phi}^2 - \bar{\phi}^2(1-\bar{\phi}^2)\right]q = 0, \tag{3.1}$$

with the boundary condition

$$(\sin^2\theta - \omega^2F^2)\frac{\mathrm{d}q}{\mathrm{d}z} + \left(\Gamma + \mathrm{i}\frac{k_y}{\sin\theta}\right)\omega^2F^2\cos\theta q = 0 \quad \text{at } z = 0. \tag{3.2}$$

For small $F/\sin\theta$, (3.1) reduces at leading order in F (assuming $k_yF = 0(1)$ and $\Gamma F = 0(1)$ to keep the maximum number of terms in the equation) to

$$\frac{\mathrm{d}^2 q}{\mathrm{d}z^2} - 2\frac{\beta_z}{\beta}\frac{\mathrm{d}q}{\mathrm{d}z} + \kappa_x^2(M_g^2\beta^2 - 1)q = 0, \tag{3.3}$$

where

$$\beta = U(z) - \frac{\omega}{k_x}, \tag{3.4a}$$

$$\kappa_x = \frac{k_x}{\sin\theta}, \tag{3.4b}$$

$$M_g^2 = M^2 + \Gamma^2F^2 + \frac{k_y^2F^2}{\sin^2\theta}, \tag{3.4c}$$

while the boundary condition is just

$$\frac{\mathrm{d}q}{\mathrm{d}z}(z=0) = 0. \tag{3.5}$$

The above (3.3) is exactly the equation we obtain for two-dimensional modes ($k_y = 0$) when the fluid is unstratified for any θ, or when $\Gamma = 0$ and $\theta = \pi/2$ for any F, that is, when the stratification plays no role. The above reduction therefore has strong implications for the instability mechanism in the strongly stratified limit. In this limit, the boundary layer stability is then equivalent to the stability of two-dimensional perturbations in a non-stratified compressible boundary layer. Note also that we are in an isothermal configuration (because we have assumed c_s uniform). The instability is therefore expected to be due to the 'acoustic modes' only. In particular, the so-called first mode of a compressible boundary layer is not expected to be present (Mack 1969).

As the angle θ has disappeared from (3.3), the dependence of the stability properties with respect to θ is entirely contained in the change of variables (3.4*a–c*). These equations tell us that the streamwise phase velocity ω/k_x is a function of κ_x and M_g only. This means that the complex frequency ω can be written as

$$\omega = \omega_{\pi/2}(\kappa_x, M_g)\sin\theta, \tag{3.6}$$

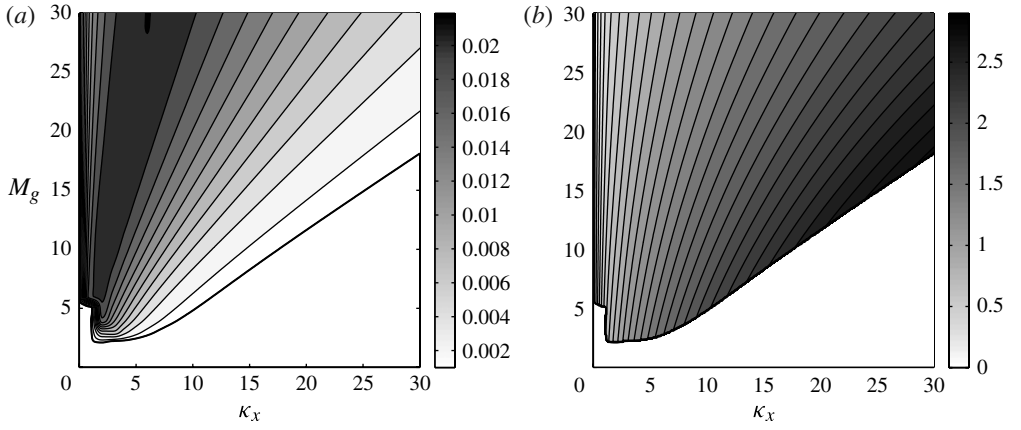

FIGURE 2. Characteristics of the most unstable mode in the limit of small F as functions of M_g and κ_x for $\theta = \pi/2$. (a) Contours of the growth rate $\mathrm{Im}(\omega_{\pi/2})$. ($b$) Contour of the oscillation frequency $\mathrm{Re}(\omega_{\pi/2})$. In both plots, the marginal stability curve is indicated by a thick solid line.

where $\omega_{\pi/2}$ is the frequency obtained for $\theta = \pi/2$. Figure 2 provides the contour levels of $\mathrm{Im}(\omega_{\pi/2})$ and $\mathrm{Re}(\omega_{\pi/2})$ in the (κ_x, M_g) plane. Using (3.4) and (3.6), these plots provide the growth rate and the oscillation frequency of the most unstable mode for any M, Γ, k_x, k_y and θ provided that $F/\sin\theta$ is small. The curve of marginal stability, indicated as a thick black line, corresponds to the contour of zero growth rate.

Figure 2(a) shows that the general Mach number M_g has to be larger than $M_c \approx 2.2$ for instability. It is interesting to note that this critical Mach number is very close to the value obtained by Mack (1969) for the destabilization of the first two-dimensional acoustic mode in an adiabatic Blasius boundary layer. In view of the definition (3.4c) of the general Mach number, this condition is reached when, for instance, the flow is strongly supersonic, $M > M_c$, non-Boussinesq effects are important, $\Gamma F > M_c$, or the perturbations are three-dimensional with $\tilde{k}_y = k_y F/\sin\theta > M_c$. In fact, whatever the Mach number M and the value of Γ, the flow is always unstable to perturbations satisfying

$$k_y^2 F^2 > \sin^2\theta (M_c^2 - M^2 - \Gamma^2 F^2). \tag{3.7}$$

Figure 2(a) tends to show that the maximum growth rate is obtained when both M_g and κ_x go to infinity with a fixed ratio M_g/κ_x. This is confirmed in figure 3, where we have plotted the maximum growth rate and the oscillation frequency versus M_g/κ_x for various κ_x. We clearly see that the curves tend to a limit curve indicated with a thick line as κ_x goes to ∞. This curve can be obtained by performing an asymptotic analysis of (3.3) as $\kappa_x \to \infty$ with $M_g/\kappa_x = O(1)$. Such an analysis has already been performed by Le Dizès & Riedinger (2010) for Taylor–Couette flow. When $\kappa_x \to \infty$, the most unstable mode is selected by its behaviour close to the boundary, and determining its structure requires a rescaling of the spatial variable. Introducing the new variables

$$\tilde{z} = \kappa_x z, \tag{3.8a}$$

$$\tilde{M}_g = \frac{U_z(0) M_g}{\kappa_x}, \tag{3.8b}$$

$$\omega_1 = \omega/(U_z(0)\sin\theta), \tag{3.8c}$$

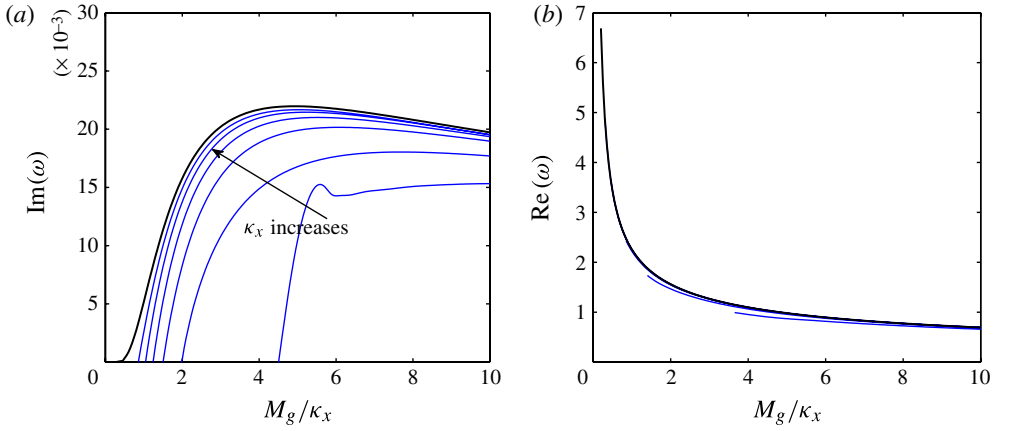

FIGURE 3. (Colour online) Characteristics of the most unstable mode in the limit of small $F/\sin\theta$ as a function of M_g/κ_x for $\theta = \pi/2$ and different κ_x ($\kappa_x = 1, 2, 5, 10, 20, 50$). The curve obtained in the limit $\kappa_x \to \infty$ is indicated by a black thick line. (*a*) Maximum growth rate $\mathrm{Im}(\omega)$. (*b*) Oscillation frequency $\mathrm{Re}(\omega)$.

equation (3.3) becomes at leading order in $1/\kappa_x$

$$\frac{\mathrm{d}^2 q}{\mathrm{d}\tilde{z}^2} - \frac{2}{\tilde{z} - \omega_1}\frac{\mathrm{d}q}{\mathrm{d}\tilde{z}} + [\tilde{M}_g^2 (\tilde{z} - \omega_1)^2 - 1]q = 0. \tag{3.9}$$

This equation depends on a single parameter $\tilde{M}_g$. Note in particular that the boundary layer profile only appears via a scaling parameter $U_z(0)$. The present analysis thus applies to any boundary layer flow provided that $U_z(0)$ is non-zero. Here, we have $U_z(0) = 1$. The most unstable mode over all $\tilde{M}_g$ is obtained for $\tilde{M}_g \approx 4.9$ and the corresponding eigen-frequency is $\omega_1 \approx 0.9909 + 0.0220\mathrm{i}$.

In practice, the base flow parameters M and Γ are fixed. Making $M_g \to \infty$ is then only possible by considering large k_y such that we have $\tilde{M}_g \sim U_z(0) F k_y/k_x$. The present analysis then tells us that, whatever the boundary layer profile, for small F, the maximum growth rate is reached for large k_x and large k_y such that $k_y/k_x \sim 4.9/(FU_z(0))$ for any fixed M, Γ and θ (provided $\theta \neq 0$). The frequency of the most unstable mode does not depend on M and Γ but varies with θ according to $\omega \sim (0.99 + 0.022\mathrm{i})U_z(0)\sin\theta$. The spatial structure (pressure fluctuation) of the most unstable mode is plotted in figure 4. The radiative structure is clearly visible in this plot. Note that the cross-stream wavenumber k_z that can be evaluated from figure 4 is approximately $k_z \approx 10\pi\kappa_x = 10\pi k_x/\sin\theta$, whereas $k_y \approx 4.9 k_x/(FU_z(0))$. The wavenumber k_z is therefore larger than k_x but smaller than k_y. This also demonstrates that the ratio $k_z/k_x \simeq 1/\sin(\theta)$ is strongly dependent on the inclination angle, whereas the ratio $k_y/k_x \simeq 1/F$ only depends on F.

4. The weakly stratified limit (large F)

When F is large, that is, when the flow is only weakly stratified, the instability does not disappear. This was first noticed for the radiative instability of a rotating potential flow (see Le Dizès & Riedinger 2010). For large F, the unstable modes tend to be localized near the boundary. As in the previous section, these modes can be captured by performing a local asymptotic analysis near $z = 0$. If we introduce

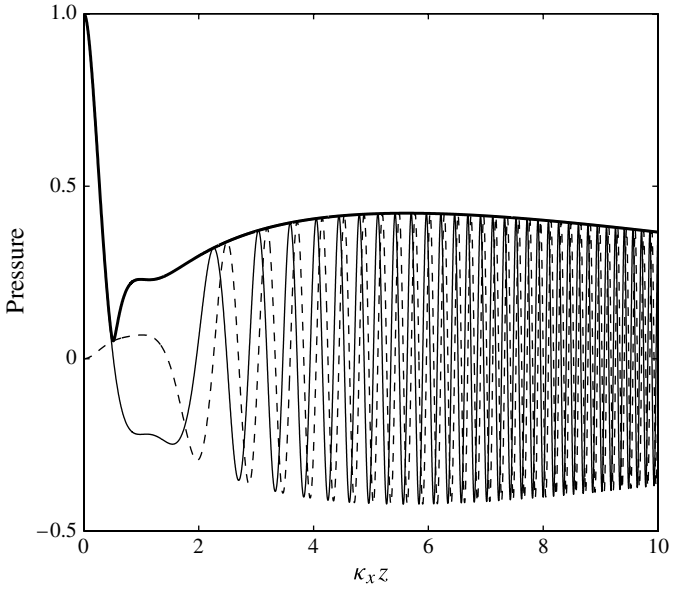

FIGURE 4. Eigenfunction (pressure amplitude) of the most unstable mode (obtained for $\tilde{M}_g \approx 4.9$ by the large κ_x and large M_g analysis) when $F/\sin\theta \ll 1$. Absolute value (thick solid line); real part (solid line); imaginary part (dashed line).

the local variable $\bar{z} = k_x U_z(0) F z$, (2.7) becomes, at leading order in $1/F$, an equation where the dependence with respect to the base flow has disappeared:

$$(\zeta^2 - \sin^2\theta)\frac{\mathrm{d}^2 p}{\mathrm{d}\bar{z}^2} + \left(2\frac{-\zeta^4 + (2\zeta^2-1)\sin^2\theta}{\zeta(\zeta^2-1)} - 2\mathrm{i}R_k \sin\theta\cos\theta\right)\frac{\mathrm{d}p}{\mathrm{d}\bar{z}} + \left(\frac{2\mathrm{i}R_k \sin\theta\cos\theta(2\zeta^2-1)}{\zeta(\zeta^2-1)} + R_k^2(\cos^2\theta - \zeta^2) + \frac{2\cos\theta\zeta^3}{\zeta^2-1}\bar{\Gamma} - \bar{\Gamma}^2\zeta^2 + \bar{M}^2\zeta^2(\zeta^2-1)\right)p = 0, \tag{4.1}$$

where

$$\zeta = \bar{z} - \omega_1, \tag{4.2}$$

and

$$\omega_1 = \omega F, \tag{4.3a}$$

$$R_k = \frac{k_y}{k_x F U_z(0)}, \tag{4.3b}$$

$$\bar{\Gamma} = \frac{\Gamma}{F k_x U_z(0)}, \tag{4.3c}$$

$$\bar{M} = \frac{M}{F^2 k_x U_z(0)}. \tag{4.3d}$$

The boundary condition reads

$$(\sin^2\theta - \omega_1^2)\frac{\mathrm{d}p}{\mathrm{d}\bar{z}} + (\mathrm{i}R_k \sin\theta\cos\theta + \bar{\Gamma}\omega_1^2\cos\theta)p = 0 \quad \text{at } \bar{z} = 0. \tag{4.4}$$

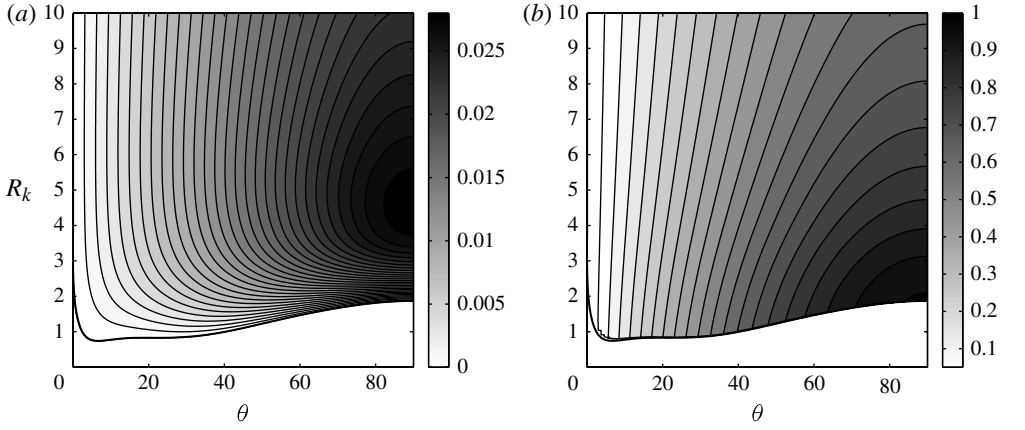

FIGURE 5. Characteristics of the most unstable mode in the limit of large F in the (θ, R_k) plane for $\bar{M} = \bar{\Gamma} = 0$. (*a*) Growth rate $\mathrm{Im}(\omega_1)$. (*b*) Oscillation frequency $\mathrm{Re}(\omega_1)$.

In the large F limit, the eigenvalue problem still depends on four parameters R_k, $\bar{\Gamma}$, $\bar{M}$ and θ, but the parameters F and k_x are no longer present. Moreover, as in the strongly stratified limit, the problem does not depend on the form of the boundary layer profile. The analysis therefore applies to any boundary layer flow, the only restriction being $U_z(0) \neq 0$.

We now consider the particular case $\bar{M} = \bar{\Gamma} = 0$. This case corresponds to situations where M and Γ are of order one or smaller, which is clearly verified in all atmospheric applications. The characteristics of the most unstable mode are plotted as a function of the two other parameters R_k and θ in figure 5. The growth rate contours are shown in figure 5(*a*) and the oscillation frequency contours are shown in figure 5(*b*). A cross-section of these $\mathrm{Im}(\omega_1)$ and $\mathrm{Re}(\omega_1)$ contour levels at $\theta = \pi/2$ is shown as a thick black line in figure 6(*a*,*b*) respectively. In these figures we have also plotted against R_k the rescaled growth rate and oscillation frequency obtained for finite F from the general (2.7). We can see that the growth rate and oscillation frequency curves do converge when F increases to the large F curves obtained from (4.1). This constitutes a validation of the asymptotic approach.

The characteristics of the most unstable mode over all R_k are indicated in figure 7 as a function of θ. It is important to note that there is apparently no non-zero critical angle below which the flow becomes stable. As shown in figure 7(*a*), the maximum growth rate vanishes at $\theta = 0$ but is strictly positive for all non-zero angles. It increases monotonously with θ to reach its maximum value for $\theta = \pi/2$ rad, that is, for the case of the flow on a vertical surface. Note that the oscillation frequency of the most unstable mode also increases with θ (see figure 7*a*), but the ratio R_k maximizing the instability decreases with θ (see figure 7*b*).

The spatial structure (pressure amplitude) of the most unstable mode for $\theta = \pi/2$ is shown in figure 8. It is interesting to compare this plot with the structure of the most unstable mode for small F shown in figure 4. In contrast with the small F case, the pressure amplitude of the most unstable mode does not exhibit oscillations away from the boundary.

5. General case ($F = O(1)$)

For fixed values of F, the problem depends on four base flow parameters F, M, Γ and θ and two perturbation parameters k_x and k_y, and could *a priori* be difficult to

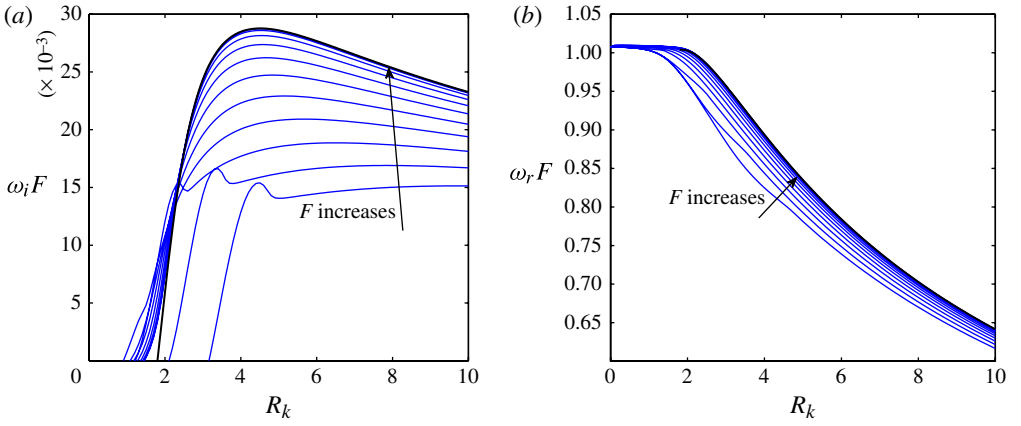

FIGURE 6. (Colour online) Characteristics of the most unstable mode versus R_k for $\bar{M} = \bar{\Gamma} = 0$ and $\theta = \pi/2$ rad and different values of F ($F = 1$, 1.11, 1.25, 1.42, 1.66, 2, 2.5, 3.33, 5, 10, 100). (a) Rescaled maximum growth rate $\mathrm{Im}(F\omega)$. (b) Rescaled oscillation frequency $\mathrm{Re}(F\omega)$.

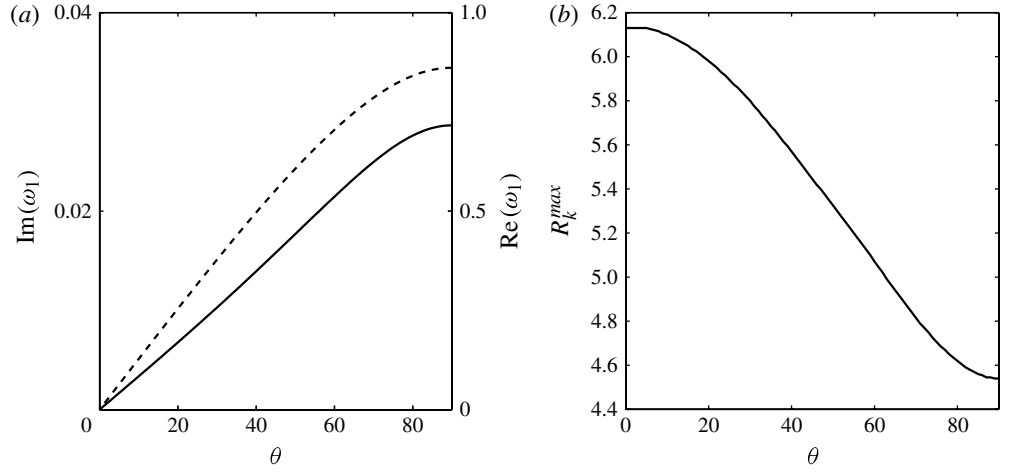

FIGURE 7. Characteristics of the most unstable mode over all R_k as a function of θ (in degree) in the limit of large F for $\bar{M} = \bar{\Gamma} = 0$. ($a$) Maximum growth rate $\mathrm{Im}(\omega_1)$ (solid line with left axis) and oscillation frequency $\mathrm{Re}(\omega_1)$ (dashed line with right axis). (b) Maximizing ratio R_k^{max}.

simplify. To limit the parameter space, we have considered configurations where both compressibility and non-Boussinesq effects are negligible, and have therefore assumed that both M and Γ can be taken equal to zero. Such a configuration is realistic for atmospheric applications where Γ and M are generally small.

For small F (§ 3), we have observed that the maximum growth rate is obtained when both k_x and k_y are large. For large F, we have seen that the stability characteristics do not depend on the values of k_x and k_y but on the ratio k_y/k_x only. It is then natural to assume that the most unstable mode is also obtained for large k_x and k_y when $F = O(1)$. This hypothesis permits us to use a reduced equation which is similar

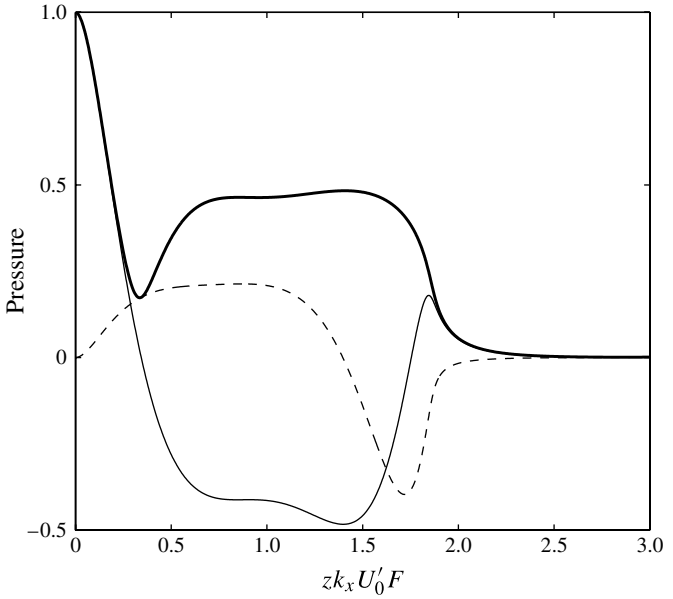

FIGURE 8. Eigenfunction (pressure amplitude) of the most unstable mode in the limit of large F for $\bar{M} = \bar{\Gamma} = 0$ and $\theta = \pi/2$. Absolute value (thick solid line); real part (solid line); imaginary part (dashed line).

to (4.1), albeit an additional term of the form $(1-\zeta^2)/(U_z(0)F)^2$. For $M = \Gamma = 0$, the problem then only depends on θ, F and the ratio k_y/k_x, and is described by the equation

$$(\zeta^2 - \sin^2\theta)\frac{\mathrm{d}^2 p}{\mathrm{d}\zeta^2} + \left(2\frac{-\zeta^4 + (2\zeta^2-1)\sin^2\theta}{\zeta(\zeta^2-1)} - 2\mathrm{i}R_k \sin\theta\cos\theta\right)\frac{\mathrm{d}p}{\mathrm{d}\zeta} + \left(\frac{2\mathrm{i}R_k\sin\theta\cos\theta(2\zeta^2-1)}{\zeta(\zeta^2-1)} + R_k^2(\cos^2\theta - \zeta^2) - \frac{1}{\bar{F}^2}(\zeta^2-1)\right)p = 0, \quad (5.1)$$

where

$$\zeta = k_x U_z(0) F z - \omega F, \quad (5.2a)$$

$$R_k = \frac{k_y}{k_x F U_z(0)}, \quad (5.2b)$$

$$\bar{F} = U_z(0)F. \quad (5.2c)$$

The condition at the boundary can be deduced from (4.4).

In figure 9, we have plotted the growth rate and oscillation frequency contours of the most unstable mode in the (θ, R_k) plane for $\bar{F} = 1$. We can see that pictures similar to the small F case (figure 5) are obtained. The maximum growth rate is obtained for $\theta = \pi/2$ and decreasing θ is stabilizing as for large F and small F.

The variation of the characteristics of the most unstable mode with respect to F are plotted in figure 10 for different values of θ. In these plots, the small F and large F predictions obtained in the two previous sections are also indicated. We can see that these asymptotic laws match very well the general numerical results for both small and large F.

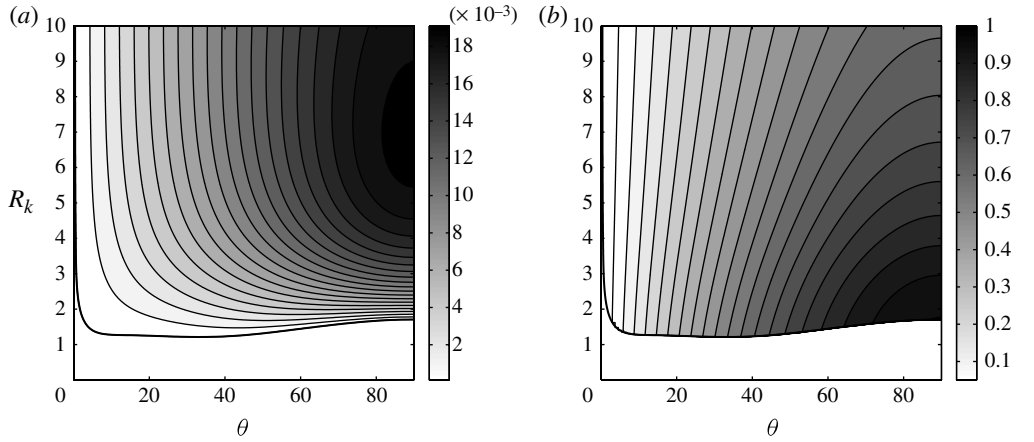

FIGURE 9. Characteristics of the most unstable mode in the (θ, R_k) plane for $\bar{F} = 1$ and $\bar{M} = \bar{\Gamma} = 0$. (*a*) Maximum growth rate $\mathrm{Im}(\omega)$. (*b*) Oscillation frequency $\mathrm{Re}(\omega)$.

The effect of the inclination angle is also visible in this figure. We clearly see in figure 10(*a*) that decreasing θ is stabilizing for any F. For $\theta = 0$, the boundary layer becomes neutrally stable for any F.

6. Conclusion

We have analysed the inviscid stability of a stably stratified compressible boundary layer flow when the boundary surface is inclined with respect to the isodensity levels. Our main result is to have proved that the boundary layer flow is unstable with respect to inviscid perturbations as soon as the surface is inclined with respect to the horizontal. Although the numerical results have been obtained for a specific velocity profile, we have also shown that the instability characteristics do not depend on the precise form of the boundary layer profile as long as it is not inflectional and with a non-vanishing shear rate at the boundary ($U_z(0) \neq 0$). In particular, the results apply to the Blasius boundary layer profile as well as other more realistic local boundary layer profiles. The growth rate of the most unstable mode has been shown to increase with the inclination angle to reach its maximum for a vertical surface $\theta = \pi/2$. The unstable modes have been shown to be three-dimensional and to correspond to large wavenumbers. In the weakly stratified limit, when both compressible and non-Boussinesq effects are negligible, both the oscillation frequency and the growth rate have been shown to scale with the Brunt–Väisälä frequency N. In the strongly stratified limit, frequency and growth rate become independent of the Froude number. Moreover, as long as the inclination angle is not too small (such that $F/\sin\theta \ll 1$), these quantities become proportional to the sine of the inclination angle. In the strongly stratified limit, compressible and non-Boussinesq effects can be easily taken into account. We have shown that they do not modify the instability nor the characteristics of the most unstable modes.

We can try to apply the results to a real configuration encountered in the atmosphere. Consider a stable nocturnal atmospheric boundary layer as reported in Frehlich, Meillier & Jensen (2008). These authors measured the following characteristics: $U_0 = 10$ m s^{-1}, $L = 100$ m, $H = 10$ km, from which we can deduce $N = 0.031$ rad s^{-1},

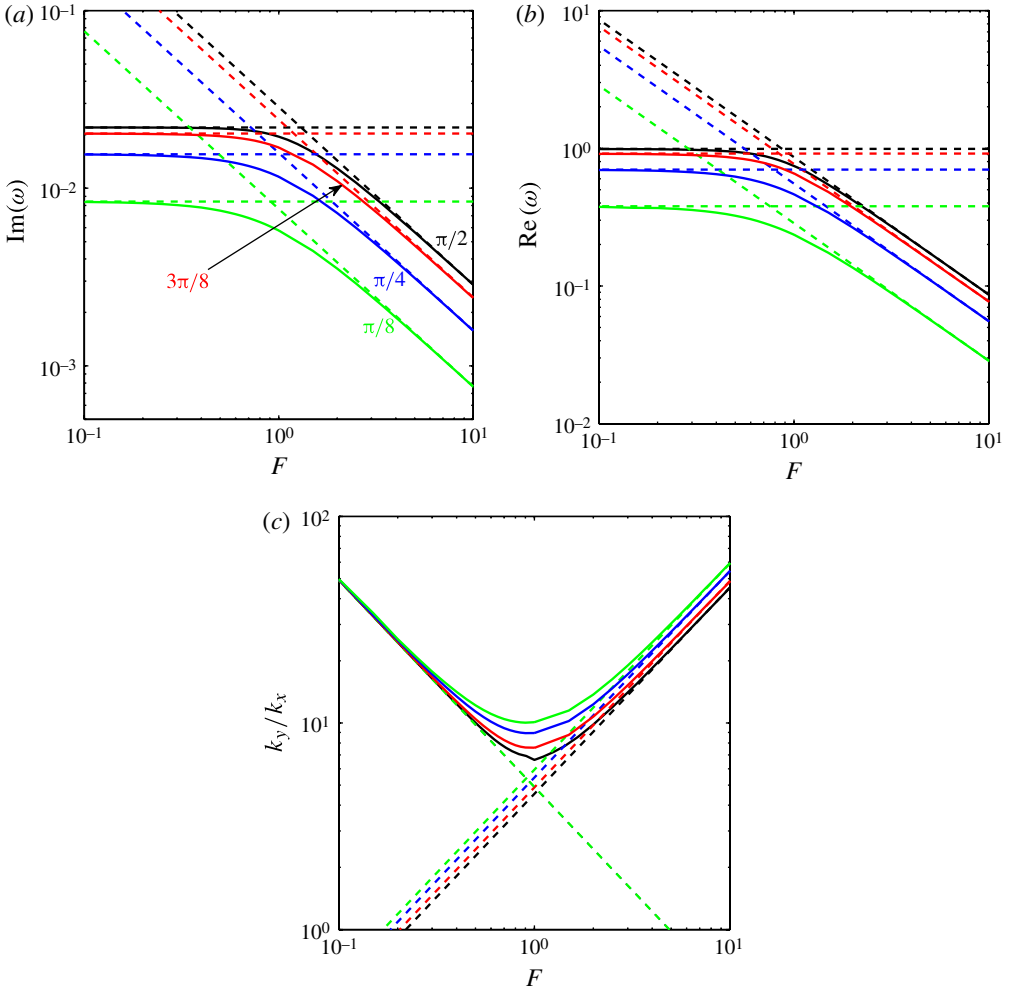

FIGURE 10. (Colour online) Characteristics of the most unstable mode over all k_y/k_x as a function of F for $\bar{M} = \bar{\Gamma} = 0$ and $\theta = \pi/8, \pi/4, 3\pi/8, \pi/2$. (*a*) Maximum growth rate $\mathrm{Im}(\omega)$. (*b*) Oscillation frequency $\mathrm{Re}(\omega)$. (*c*) Maximizing ratio k_y/k_x. The dotted lines are the predictions obtained from small and large F analyses.

and the Froude number $F \approx 3.2$. We can verify that compressible and non-Boussinesq effects are small: $M \approx 0.03$, $\Gamma \approx 0.01$. Both global rotation and viscosity are also negligible as the Rossby number is $Ro = U_0/(Lf) \approx 1000$, and the Reynolds number $Re = U_0 L/\nu \approx 10^8$ (with $\nu = 10^{-5}$ m^2 s^{-1} and $f = 10^{-4}$ s^{-1} at mid-latitude). If the boundary layer was inclined at an angle $\theta = \pi/8$ rad, we would obtain the following characteristics for the most unstable mode: $\omega = (0.0088 + \mathrm{i}0.00024)$ rad s^{-1}, and $k_y/k_x = 20$. Both the period $T = 2\pi/\omega_r \approx 12$ min, and the growth time $\tau = 1/\omega_i \approx 69$ min of the most unstable mode would then be compatible with the 12-hour period of occurrence of the flow. Moreover, the viscous cut-off length, which can be estimated from $L_\nu = \sqrt{\nu/\omega_i} \approx 0.2$ m, would also be much smaller than L. The shortest wavelength of the most unstable mode would not be expected to be smaller than L. This would give a spanwise wavelength $\lambda_y \approx 100$ m, and a streamwise wavelength $\lambda_x = 20\lambda_y \approx 2000$ m. In conclusion, the stable atmospheric boundary layer reported

in Frehlich *et al.* (2008) would be unstable by a long streamwise wavelength mode if its boundary surface was inclined at 22.5°. This particular example demonstrates that this instability could be active in the atmosphere, even for relatively small inclination angles. It would be interesting to confirm this prediction with real data.

In this paper, we have not considered viscous or diffusion effects. Although these effects are expected to be stabilizing on the present instability, they are also known to be a source of instability in boundary layers. In a homogeneous fluid, the growth rate of viscous modes (Tollmien–Schlichting waves) scales as $Re^{-1/2}$ (Drazin & Reid 1981). These modes are thus expected to remain less unstable than the inviscid modes found here for sufficiently large Reynolds numbers. However, in the large-Reynolds-number limit, the boundary layer also becomes extremely sensitive to external perturbations which can transiently grow and be responsible for the boundary layer (by-pass) transition (Schmid & Henningson 2001). How these transient behaviours are affected by stable stratification and compete with the inviscid instability described here remains an interesting open issue (see Bakas & Farrell 2009). Moreover, we do not know the nonlinear evolution of the present radiative instability and whether it can lead to a boundary layer transition and/or enhance mixing near the wall.

REFERENCES

Bakas, N. A. & Farrell, B. F. 2009 Gravity waves in a horizontal shear flow. Part II. Interaction between gravity waves and potential vorticity perturbations. *J. Phys. Oceanogr.* **39**, 497–511.

Balmforth, N. J. 1999 Shear instability in shallow water. *J. Fluid Mech.* **387**, 97–127.

Basovich, A. Y. & Tsimring, L. S. 1984 Internal waves in a horizontally inhomogeneous flow. *J. Fluid Mech.* **142**, 223–249.

Billant, P. & Le Dizès, S. 2009 Waves on a columnar vortex in a strongly stratified fluid. *Phys. Fluids* **21**, 106602.

Broadbent, E. & Moore, D. W. 1979 Acoustic destabilization of vortices. *Phil. Trans. R. Soc.* A **290**, 353–371.

Candelier, J. 2010 Instabilités radiatives des jets et couches limites atmosphériques. PhD thesis, Aix-Marseille Université, Marseille.

Candelier, J., Le Dizès, S. & Millet, C. 2011 Shear instability in a stratified fluid when shear and stratification are not aligned. *J. Fluid Mech.* **685**, 191–201.

Chimonas, G. 1974 Consideration of the stability of certain heterogeneous shear flows including some inflexion-free profiles. *J. Fluid Mech.* **65**, 65–69.

Chimonas, G. 2002 On internal gravity waves associated with the stable boundary layer. *Boundary-Layer Meteorol.* **102**, 139–155.

Churilov, S. M. 2005 Stability analysis of stratified shear flows with a monotonic velocity profile without inflection points. *J. Fluid Mech.* **539**, 25–55.

Churilov, S. M. 2008 Stability analysis of stratified shear flows with a monotonic velocity profile without inflection points. Part 2. Continuous density variation. *J. Fluid Mech.* **617**, 301–326.

Davis, P. A. & Peltier, W. R. 1976 Resonant parallel shear instability in the stratified planetary boundary layer. *J. Atmos. Sci.* **33**, 1287–1300.

Drazin, P. G. & Reid, W. H. 1981 *Hydrodynamic Stability*. Cambridge University Press.

Dritschel, D. G. & Vanneste, J. 2006 Instability of a shallow-water potential-vorticity front. *J. Fluid Mech.* **561**, 237–254.

Dunn, W. & Lin, C. 1955 On the stability of the laminar boundary layer in a compressible fluid. *J. Aero. Sci.* **22**.

Eckart, C. 1960 *Hydrodynamics of Oceans and Atmospheres*. Pergamon.

Ford, R. 1994 The instability of an axisymmetric vortex with monotonic potential vorticity in rotating shallow water. *J. Fluid Mech.* **280**, 303–334.

FREHLICH, R., MEILLIER, Y. & JENSEN, M. L. 2008 Measurements of boundary layer profiles with in situ sensors and Doppler lidar. *J. Atmos. Ocean. Technol.* **25**, 1328–1340.

GOSSARD, E. E. & HOOKE, W. H. 1975 *Waves in the Atmosphere*. Elsevier.

HOUGHTON, J. T. 1986 *The Physics of Atmosphere*. Cambridge University Press.

HOWARD, L. N. 1961 Note on a paper of John W. Miles. *J. Fluid Mech.* **10**, 509–512.

KOPEV, V. F. & LEONTEV, E. A. 1983 Acoustic instability of an axial vortex. *Sov. Phys. Acoust.* **29**, 111–115.

LE DIZÈS, S. & BILLANT, P. 2009 Radiative instability in stratified vortices. *Phys. Fluids* **21**, 096602.

LE DIZÈS, S. & RIEDINGER, X. 2010 The strato-rotational instability of Taylor–Couette and Keplerian flows. *J. Fluid Mech.* **660**, 147–161.

LEES, L. & LIN, C. C. 1946 Investigation of the stability of the laminar boundary layer in a compressible fluid. NACA Technical Note 1115.

LEES, L. & RESHOTKO, E. 1962 Stability of the compressible laminar boundary layer. *J. Fluid Mech.* **12**, 555–590.

LINDZEN, R. S. & BARKER, J. W. 1985 Instability and wave over-reflection in stably stratified shear flow. *J. Fluid Mech.* **151**, 189–217.

LUO, K. H. & SANDHAM, N. D. 1997 Instability of vortical and acoustic modes in supersonic round jets. *Phys. Fluids* **9**, 1003–1013.

MACK, L. M. 1965 The stability of the compressible laminar boundary layer according to a direct numerical solution. In *Recent Developments in Boundary Layer Research*, *AGARDograph*, vol. 97, pp. 329–362.

MACK, L. M. 1969 Boundary layer stability theory. *Tech. Rep.* JPL-900-277-REV-A, Jet Propulsion Laboratory.

MACK, L. M. 1990 On the inviscid acoustic-mode instability of supersonic shear flows. Part 1. Two-dimensional waves. *Theor. Comput. Fluid Dyn.* **2**, 97–123.

MASTRANTONIO, G., EINAUDI, F., FUA, D. & LALAS, D. P. 1976 Generation of gravity waves by jet streams in the atmosphere. *J. Atmos. Sci.* **33**, 1730–1738.

MILES, J. W. 1961 On the stability of heterogeneous shear flows. *J. Fluid Mech.* **10**, 496–508.

PARRAS, L. & LE DIZÈS, S. 2010 Temporal instability modes of supersonic round jets. *J. Fluid Mech.* **660**, 173–196.

RIEDINGER, X., LE DIZÈS, S. & MEUNIER, P. 2010*a* Viscous stability properties of a Lamb–Oseen vortex in a stratified fluid. *J. Fluid Mech.* **645**, 255–278.

RIEDINGER, X., LE DIZÈS, S. & MEUNIER, P. 2011 Radiative instability of the flow around a rotating cylinder in a stratified fluid. *J. Fluid Mech.* **672**, 130–146.

RIEDINGER, X., MEUNIER, P. & LE DIZÈS, S. 2010*b* Instability of a vertical columnar vortex in a stratified fluid. *Exp. Fluids* **49**, 673–681.

SATOMURA, T. 1981 An investigation of shear instability in a shallow water. *J. Met. Soc. Japan* **59**, 148–167.

SCHECTER, D. A. & MONTGOMERY, M. T. 2004 Damping and pumping of a vortex Rossby wave in a monotonic cyclone: critical layer stirring versus inertia–buoyancy wave emission. *Phys. Fluids* **16**, 1334–1348.

SCHMID, P. J. & HENNINGSON, D. S. 2001 Stability and transition in shear flows. In *Applied Mathematical Sciences*, vol. 142. Springer.

SMYTH, W. & PELTIER, W. 1989 The transition between Kelvin–Helmholtz and Holmboe instability: an investigation of the overreflection hypothesis. *J. Atmos. Sci.* **46** (24), 3698–3720.

TAKEHIRO, S.-I. & HAYASHI, Y.-Y. 1992 Over-reflection and shear instability in a shallow-water model. *J. Fluid Mech.* **236**, 259–279.

TAM, C. K. W. & HU, F. Q. 1989*a* The instability and acoustic wave modes of supersonic mixing layers inside a rectangular channel. *J. Fluid Mech.* **203**, 51–76.

TAM, C. K. W. & HU, F. Q. 1989*b* On the three families of instability waves of high-speed jets. *J. Fluid Mech.* **201**, 447–483.

WATADA, S. 2009 Radiation of acoustic and gravity waves and propagation of boundary waves in the stratified fluid from a time-varying bottom boundary. *J. Fluid Mech.* **627**, 361–377.